Ninth International Conference on
THIN-WALLED STRUCTURES – ICTWS2023
Sydney, Australia, Nov 29 – Dec 1, 2023

A SMART STRUCTURAL ANALYSIS METHOD TO AXIAL COMPRESSION COLD-FORMED C-SECTION MEMBERS (ICTWS2023)

Xi Zhao*, Pengfei Du*, Yanxia Zhang* and Hanbo Guan**

* Beijing University of Civil Engineering and Architecture
e-mails: zhaoxi@bucea.edu.cn, dupengfei723@163.com,zhangyanxia@bucea.edu.cn

** Beijing Intelligent Prefabricated Building Research Institute
e-mail: dug@biipb.org.cn

Keywords: Cold formed steel, Finite element model, Machine learning, Smart structural analysis.

Abstract. *Cold-formed steel is widely used in the construction of buildings and infrastructure due to its high strength and lightweight properties. However, its thin-walled structure makes it sensitive to geometric loading capacity, specifically in compression capacities. Consequently, the design methods of thin-walled cold-formed steel structures have been developed through simulation-based or performance-based designs. However, an ongoing challenge in these trending design methods is improving the efficiency and accuracy of member-level and system-level numerical simulations. In recent years, machine learning methods have rapidly developed and offer potential solutions for predicting structural performance, such as the loading capacity of cold-formed steels rapidly and robustly. In this context, the authors propose a smart structural analysis algorithm that trains a surrogate model of axial-compression cold-formed steel members through high-fidelity finite element analysis. The finite element models are validated through a series of axial-compression tests of cold-formed steel members, where parameters like meshing, boundaries, and other finite-element properties are confirmed. Input data, such as geometric and material properties, are utilized to generate training targets for peak structural performance, such as peak loads. The surrogate model provides a vital design parameter linked to geometric dimensions and materials properties. Normalizing the variables of the surrogate model in advance enhances its efficiency. Parametric analysis is carried out in advance to enable substantially reduced training sample sizes while maintaining high learning efficiency. The surrogate model's reliability was validated via the classification error rating method, which fed back unto the training classification to enhance the model's accuracy and efficiency. In conclusion, the smart structural analysis algorithm has created a robust and reliable tool for analysis-based or simulation-based designs that can potentially replace traditional time-consuming numerical simulations. The new design approach can be customized and popularized in practice.*

1 INTRODUCTION

Cold-formed steel (CFS) members, manufactured at ambient temperatures, offer a host of benefits such as high strength, ease of transport, and quick installation. Their thin-walled nature, however, renders the structural performance concerning strength and stability particularly susceptible to geometric imperfections [1]. These imperfections are common occurrences during the fabrication, transportation, and storage of CFS members [2]. Therefore, accurate representation of these imperfections is vital in any numerical simulations of CFS. In conventional simulations from China and North America, buckling analysis is frequently applied to determine the first buckling mode shape. Here, the scaling factor equals the member's actual length divided by 960 [3-5]. By fusing this mode shape with the scaling factor, a preliminary representation of the CFS member's initial imperfection is achieved. However, this approach does not fully capture the authentic geometric imperfections present in the CFS member. There exists a demand for more precise measurement methods which

involve advanced visual equipment like 3D laser [6-7] and DIC [8] to capture point cloud data. This data subsequently aids in developing a realistic numerical imperfection model for CFS members.

In practical applications, the point cloud data tends to be voluminous, impacting subsequent data analysis. Additionally, converting this data into numerical models fit for mechanical performance analysis often necessitates smooth interoperation and transition among multiple software platforms [9], thereby diminishing efficiency. Moreover, setting up the numerical model parameters and undertaking the calculation process usually demand significant time and manpower resources. Though this high-precision imperfection simulation technique for CFS members carries scientific research value, its feasibility for large-scale applications in real-world engineering projects is relatively low.

The advent and continual innovation of next-gen artificial intelligence technologies, namely, machine learning and deep learning, have found extensive use in the realm of cold-formed steel [10] [11]. Pioneering researchers like Zhao [8], Xu [12], and Xiao [13] have harnessed machine learning methodologies to undertake comprehensive analyses of CFS, spanning imperfection simulation, mechanical performance prediction, to structural design optimization. Their groundbreaking studies have yielded numerous valuable, application-oriented findings. In a study conducted by Xu [12], a surrogate model was established based on a database containing 232 cold-formed stainless-steel columns to forecast the maximal load-bearing ability of these specific types of columns. The creation of this model entailed training a collection of seven machine learning techniques, including XGBoost, to delve into the complicated interdependencies between a vast array of column parameters and their corresponding maximum load tolerance. Parallel endeavours can be noted in Dissanayake's work [14], where machine learning methodologies such as support vector regression were employed to construct a surrogate model intended to predict the flexural resistance of steel infrastructure elements. These surrogate models provide precise estimations of the peak load-bearing capacity of structural members, a vital attribute in mechanical engineering. Despite this, there's a noticeable lack of comprehensive research dedicated to the full axial compression process of Cold-Formed Steel (CFS) members. It's crucial that surrogate models are trained not just to grasp figures at the ultimate stress points; they also need to comprehend the entire structural performance.

This paper aims to establish a surrogate model that can predict the complete loading process of CFS members under axial compression by analyzing and training a numerical simulation database. In Section 2, a complete input-output database is constructed by analyzing 100 CFS members with different parameters using traditional numerical simulation methods. In Section 3, a surrogate model called Fast Trend Model (FTM) is developed to accurately and quickly predict key parameters of the load-displacement curve, with the peak load being used as a validation indicator. In the final section, the reliability and robust of the model are discussed through multi-parameter analysis, and the parameterization method of the load-displacement curve is also discussed.

2 NUMERICAL MODEL

2.1 Dimension of CFS members

The selected numerical simulation model utilizes cold-formed C-section steel members. Detailed dimensions are outlined in Table 1. Five distinct lengths of CFS members are presented (Figure 1): 450mm, 1200mm, 1800mm, 2400mm, and 3000mm. The cross-sectional thicknesses (Figure 1) range from 1.5mm to 3mm, increasing in increments of 0.5mm. The flanges (Figure 1) vary in height, with five distinct measurements: 140mm,

180mm, 200mm, 240mm, and 280mm. The flange widths for all cross-sections are consistently 70mm, with the exception of the 140mm flange height, which, as per the specifications, necessitates a flange width of 60mm. Furthermore, all CFS members are equipped with a 20mm side lip. These initial geometric parameters collectively yield a total of 100 unique initial CFS members.

Table 1: Size of CFS members.

Lengths(mm)	Thicknesses(mm)	Web heights(mm)	Flange width(mm)
450	1.5	140	60
1200	2.0	180	70
1800	2.5	200	70
2400	3.0	240	70
3000		280	70

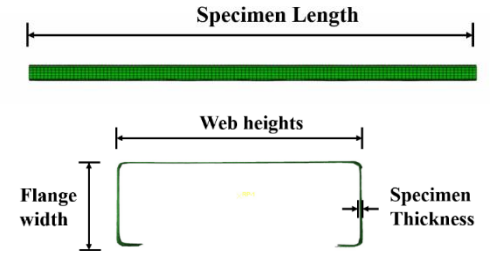

Figure 1. Size of CFS members.

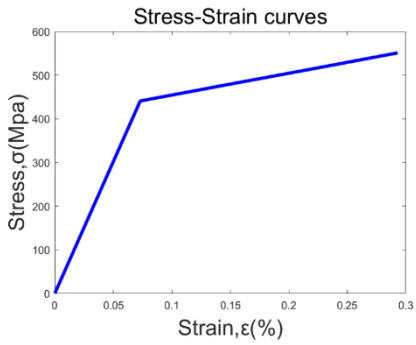

Figure 2. Stress-Strain curves.

2.2 Numerical simulation

In this study, conventional numerical methods are employed to analyze a series of axially compressed CFS members. Typically, two numerical models with identical material properties and dimensions are necessary. The first model is conducted with buckling analysis that the first-mode shape is considered as the initial geometric imperfection shape. The second model utilizes the obtained geometric imperfection shape with L/960 as the magnitudes of imperfection. A collapse analysis is conducted to the second model thereafter. The mesh elements of the models are S4R shell elements.

2.2.1 Material Properties

Given that this study primarily focuses on the initial geometric shape of the numerical model, to ensure that the material properties of the members do not influence the final analysis output, all models in this simulation are assumed to possess identical material properties. The Young's modulus is set at 196000Mpa, and the Poisson's ratio is assumed to be the standard value of 0.3 for steel. Previous numerical simulations have indicated minimal difference in the final calculation results between using a bilinear stress-strain model and a multilinear stress-strain model. Moreover, employing a bilinear stress-strain model can significantly enhance the speed of numerical simulations. This study does not conduct an in-depth analysis of material properties but utilizes a relatively simple bilinear stress-strain model, with the stress-strain table depicted in Figure 2.

2.2.2 Boundary Conditions

The boundary conditions encompass both the loading conditions and the restraint conditions, and the boundary conditions for the two numerical models are set to be identical. The boundary conditions assumed in this study are articulated, where the reference point RP1 at one end aligns with the centroid of its corresponding section. RP1 is rigidly attached to the end node of the model, permitting axial displacement and minor axial rotation of RP1. At the opposite end, another reference point RP2 is positioned at the centroid of the section, and akin to RP1, RP2 is strictly bound to the other end node of the model, allowing only minor axis rotation.

2.2.3 Analysis Step

The initial increment step is set at 0.1, the maximum increment step at 10^{36}, and the minimum increment step at 10^{-5}. The step size is typically set between 50-100, depending on the length. A step size that is too large fails to accurately capture the failure process of the model, while a step size that is too small results in computationally intensive and time-consuming calculations. Therefore, the suitable load step can be determined during the calculation process based on the trend of the calculation curve, representing the current stress state of the model.

2.2.4 Analysis results

By numerical analysis computation, the analysis results of 100 CFS members have been obtained. The failure modes of five different lengths of members are shown in **Figure 3**. Subsequently, it is necessary to read the complete stress process, including the load-displacement curve, for training and learning as a database for the surrogate model.

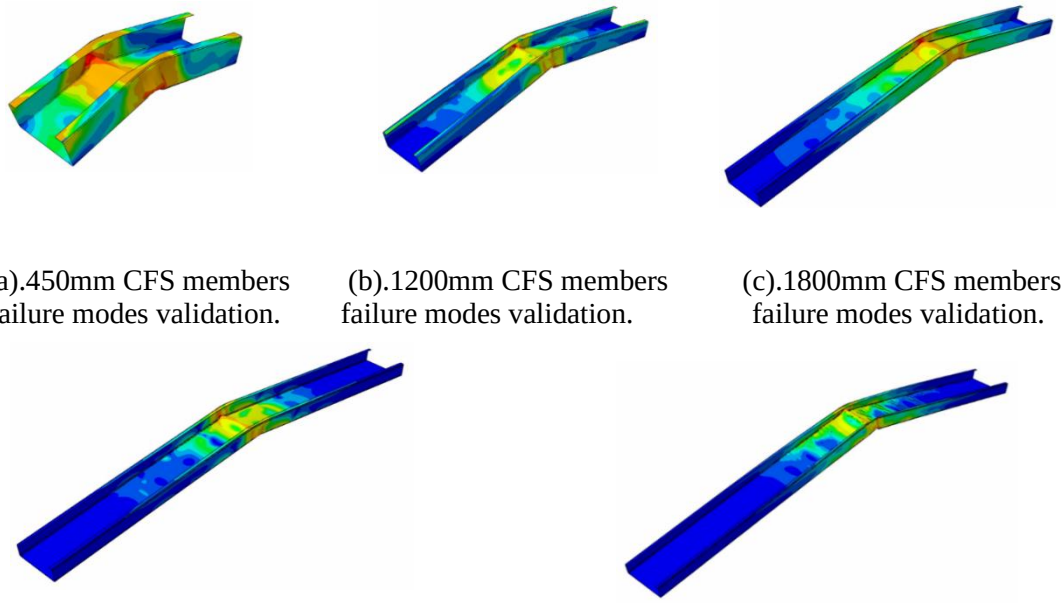

(a).450mm CFS members failure modes validation.

(b).1200mm CFS members failure modes validation.

(c).1800mm CFS members failure modes validation.

(d).2400mm CFS members failure modes validation.

(e).3000mm CFS members failure modes validation.

Figure 3. Failure modes validation.

3 MACHINE LEARNING ALGORITHM

3.1 Initial parameter analysis

In this study, the mechanical behavior of CFS members is predicted based on their initial geometric configurations. Given the substantial variances in geometric parameters across the models examined, it's imperative to perform a correlation analysis (as defined in Equation 1) among the primary geometric attributes of these numerical models. The input parameters (X) encompass the slenderness ratio (λ), length (L), section thickness (t), cross-sectional area (A), web height (H), and the ratio of web height to thickness (W). The output parameter (Y), for instance, represents peak loads. By evaluating the correlation coefficients, the three most influential geometric attributes for the training process are identified. A comparative analysis of input and output values across 100 numerical models reveals the final correlation coefficients, as detailed in Table 2.

$$\rho_{X,Y} = \frac{N\sum XY - \sum X \sum Y}{\sqrt{N\sum X^2 - (\sum X)^2}\sqrt{N\sum Y^2 - (\sum Y)^2}} \quad (1)$$

Where N is the number of samples, X is an input value, Y is an output value, and $\rho_{X,Y}$ is the correlation coefficient.

Table.2 Correlation coefficient of geometric parameters between peak loads.

Correlation coefficient	Slenderness ratio (λ)	Length (L)	Thickness (t)	Area (A)	Web height (H)	Web height to thickness ratio (W)
Peak loads	-0.5785	-0.5684	0.7589	0.6579	0.015	-0.5308

The highest correlation coefficients are between thickness and area, which are 0.7589 and 0.6579 respectively. This indicates a highly linear correlation between the cross-sectional thickness and peak load of CFS members, while the cross-sectional area shows a significant linear correlation. However, since the cross-sectional area is determined by the cross-sectional thickness, only the higher value of the correlation coefficient is considered, which is the cross-sectional thickness. In addition, the length and slenderness ratio of the CFS specimens also have a significant impact on their peak load, with correlation coefficients of -0.5785 and -0.5684 respectively. This suggests a highly negative correlation between the length and slenderness ratio of CFS member's peak load. Considering that both factors have a similar influence on the peak load of CFS members, the slenderness ratio is selected as the second geometric characteristic parameter. Finally, the correlation coefficients between the web height and the web height to thickness ratio are 0.015 and -0.5308, respectively. Clearly, the web height to thickness ratio needs to be selected. Thus, the three selected feature inputs are the slenderness ratio, thickness, and web height to thickness ratio.

3.2 Model training

In the realm of structural engineering, multiple linear regression serves as a robust statistical tool, extensively employed for data analysis and predictive modeling. This method elucidates the relationship between several independent variables and a dependent variable, utilizing the least squares fitting technique. A multiple linear regression model is formulated for predicting outputs. Utilizing MATLAB's 'fitlm' function, a potent instrument for fitting linear regression models, the relationship between features such as slenderness ratio, thickness, web height to thickness ratio, and peak load can be explored and analyzed (Equation 2). In this equation, $q, p_1, p_2,$ and p_3 represent the unknown coefficients of the model. Compared to

intricate machine learning methodologies, this approach offers advantages like rapid computational speed and comprehensibility. Thus, the 'fitlm' function is employed to ascertain the multiple linear regression correlation between the variables.

$$F_{pre} = q - p_1 \times \lambda + p_2 \times t^4 - p_2 \times \mathrm{W} \quad (2)$$

$$\Delta_{pre} = |F_{actual} - F_{pre}|/F_{actual} \quad (3)$$

When significant disparities exist between geometric parameters, it may hinder the gradient descent's progression and result in outliers during practical computations. To mitigate the final impact of these differences on model training, specific techniques are often required. In this study, due to a pronounced discrepancy between the slenderness ratio and thickness feature values, a fourth power is applied to the thickness feature value, enhancing both the convergence speed of the iterative solution and its precision.

The data for this study consists of 100 randomly selected sets, partitioned into an 80% training set and a 20% testing set. The former is utilized to train the multiple linear regression model, i.e., FTM, while the latter validates the model's accuracy. Given the importance of axial load output in cold-formed steel members' actual performance data, an additional constraint (Equation 3) is imposed, stipulating that the percentage error (Δ_{pre}) between the actual peak load (F_{actual}) and the predicted peak load (F_{pre}) must not surpass a specific threshold. Should the testing set data exceed this limit, the process must be reiterated, encompassing the re-division of training and testing sets and model retraining, until the output prerequisites are entirely satisfied. After extensive testing, it was determined that the model's optimal performance was achieved with a threshold of 15%. Consequently, a multiple regression model, i.e., FTM was derived based on slenderness ratio, thickness, and web height to thickness ratio, with q valued at 194.7, and p_1, p_2, and p_3 at 1.0568, 1.743, and 0.23777, respectively.

Through the process of model training, a definitive relationship was established between the slenderness ratio (λ), section thickness (t), web height to thickness ratio (W), and the predicted peak load (F_{pre}) of the cold-formed steel member. In the evaluation phase, 20 sets of testing data were analyzed, and remarkably, none of the percentage errors (Δ_{pre}) exceeded the 15% threshold, with an average deviation of just 6.62% (as depicted in Figure 4). This empirical evidence underscores the efficacy of the FTM model in accurately predicting the peak load, demonstrating its practical applicability in the field of structural engineering.

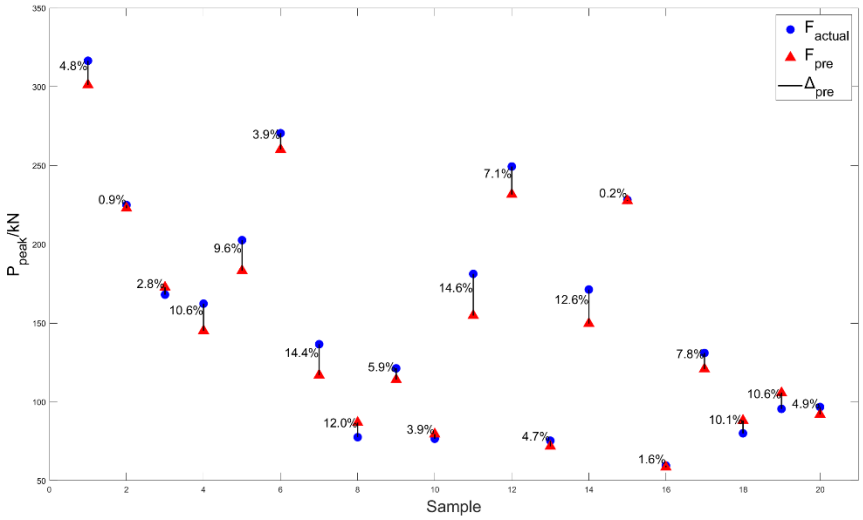

Figure 4. F_{pre} and F_{actual} of the testing set.

4 DISCUSSIONS

Despite the preliminary evaluation of the model through the test set and established thresholds, the test set's sample size is relatively small, and the evaluation methodology is somewhat limited. To address this, we will input the feature values of an expanded set of 100 sample data points into the trained FTM model. This will allow us to conduct a more comprehensive evaluation, remove outliers, and discuss the model's strengths and weaknesses. Additionally, we will delve into the parameterization methods for the load-displacement curve.

4.1 Peak loads

Upon inputting the feature values of the 100 data samples into the FTM model, a prediction for the peak load (F_{pre}) gets extrapolated. This predicted result then gets juxtaposed with the actual peak load (F_{actual}) within the sample set. As illustrated in Figure 5, the unbroken line on the graph would represent a perfect parity between F_{actual} and F_{pre}. The closeness of the data points to this line hints at the accuracy of the model's forecasts.

A significant volume of data points congregates near the unbroken line, suggesting a high degree of precision in the model's peak load predictions. However, a handful of data points exhibit substantial deviation from the actual peak load, indicating outliers within the dataset. These must be factored in when employing the model for future load forecasts.

Furthermore, the dotted line in the graph denotes the best fitting line for these samples, with a slope value of 0.8768 and an intercept of 16.30. This further reinforces the relative accuracy of the model in predicting peak loads.

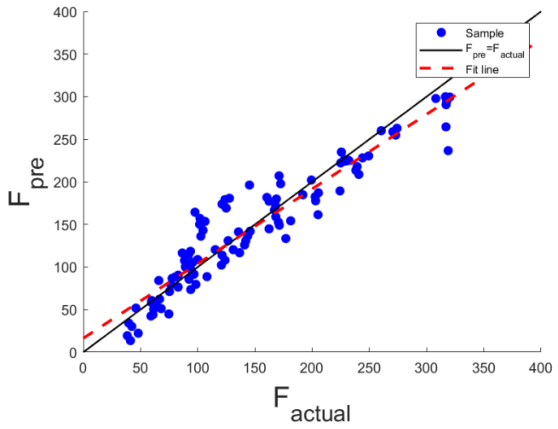

Figure 5. F_{pre} and F_{actual} for FTM model.

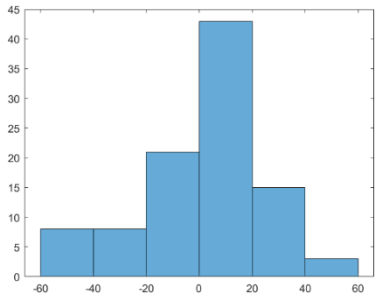

Figure 6. Residual histogram.

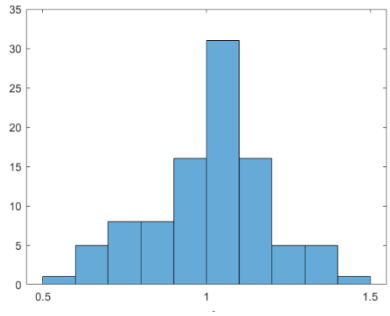

Figure 7. Ratio Histogram.

After analysing both the residuals (see Equation 4) and the ratios (Equation 5) of the predicted FTE load versus the actual load, it's evident that both these residuals (as presented in Figure 6) and ratios (depicted in Figure 7) generally follow a normal distribution trend. The 95% confidence interval of the residuals ranges from -43.8kN to 47.5kN, which is comfortably nestled within the -50kN to 50kN bracket. In a similar fashion, the 95% confidence interval for the ratios spans from 0.67 to 1.36. What these indications lead us to conclude is that there is a reliable correlation between our model's predictions and the bulk of the actual loads. Furthermore, we can assess the distribution of these predicted results as satisfactory by industry standards.

$$Residual = F_{actual} - F_{pre} \quad (4)$$

$$ratio = F_{actual}/F_{pre} \quad (5)$$

4.2 Evaluation of models

To more effectively assess the accuracy of the prediction results produced by the models, the predictive performance of the FTM model was gauged using several key metrics (as defined in Equations 6-8). These include the mean squared error (MSE), coefficient of determination (R^2), and coefficient of variation (COV) of the predicted values relative to the target values, all of which are detailed in Table 2. Initial analysis reveals that the FTM model exhibits an MSE of 2.02 and an R^2 value of 0.10, signifying a robust fit for the peak load. This leads to the conclusion that the prediction is highly accurate. With a COV value of 0.05, the FTM model further validates its commendable output dispersion. Collectively, these three

metrics underscore the FTM model's initial predictive proficiency for peak load, while also highlighting areas where optimization and enhancement are possible.

$$MSE = \frac{1}{n}\sum_{i=1}^{n}\left(F_{actual} - F_{pre}\right)^2 \tag{6}$$

$$R^2 = 1 - \frac{\sum_i\left(F_{actual} - F_{pre}\right)^2}{\sum_i\left(F_{mean} - F_{pre}\right)^2} \tag{7}$$

F_{mean} is the average value of all predicted values (F_{pre})

$$COV = \frac{\sigma_{p/A}}{\mu_{p/A}} \tag{8}$$

The $\sigma_{p/A}$ and $\mu_{p/A}$ respectively represent the average and variability of the ratio between predicted values (F_{pre}) and target values (F_{pre}).

Table 2 FTM model evaluation.

	MSE	R^2	COV
FTM	642.02	0. 910	0.05

Upon scrutinizing the graphs and metrics, it becomes evident that the FTM model, grounded in the 'fitlm' algorithm, can be trained and optimized by establishing an output threshold. It can deliver fundamental predictive performance by utilizing input feature values. While most of the predictions are accurate, the model's linear regression algorithm does impose certain limitations, such as unexpected outcomes in certain scenarios and challenges in significantly enhancing prediction accuracy. Nevertheless, the model boasts advantages like rapid computational speed and ease of comprehension, making it a fitting predictive model for crucial parameters in the axial compression process of CFS members.

Moreover, it's worth highlighting that the FTM models' fitting lines tend to predict values higher than the actual ones when the peak load is small. Conversely, the actual values surpass the predicted ones when the peak load is large. This implies that the model tends to overestimate the load when predicting smaller peak loads, and the effect is inversed for larger peak loads. Therefore, when optimizing the model and devising alternative algorithms for prediction, it's crucial to make targeted adjustments to address this characteristic.

4.3 Load-Displacement Curve

In the preceding section, we delved into the critical output of the numerical model, namely the axial compressive peak load, and established two potent prediction models based on the relationship between input and output. However, relying solely on a single peak load falls short in portraying the comprehensive stress-strain process of a CFS member. Consequently, it becomes imperative to capture the full-time stress-strain process, encompassing the load-displacement curve.

The conventional load-displacement curve is intricate and poses challenges for direct processing with machine learning techniques. Nevertheless, it can be converted into several relatively intuitive curve parameters through strategic segmentation and parameterization. Mirroring the methodology employed in training and predicting the peak load surrogate model previously discussed, a surrogate model can be trained to forecast the curve parameters grounded in the input features of the numerical model. Ultimately, by amalgamating these

parameters, the entire stress-strain curve can be constructed, enabling the prediction of the complete curve using the numerical model's input features.

For instance, a typical axial compressive load-displacement curve can be broadly segmented into three parts: the load-increasing segment, the peak load segment, and the load-decreasing segment (Figure 8a). Initially, these three segments can be parameterized and fitted individually. The load-increasing segment can be modeled as a quadratic function originating at the origin (Equation 9), characterized by parameters a and b. Likewise, the peak load segment can be conceptualized as a portion of a circular arc (Equation 10), represented by three parameters: the coordinates of the arc's center (o_x, o_y) and the radius (r). Lastly, the load-decreasing segment can be depicted as a power function (Equation 11), symbolized by parameters m and n. Through this methodology, the fitting of the entire load-displacement curve is accomplished using seven parameters.

Subsequently, a methodology akin to the one discussed earlier can be employed to train a surrogate model and delineate the relationship between the initial geometric features of the numerical model and the curve parameters. This surrogate model can predict the full set of curve parameters. Then, the parameters derived from the surrogate model can be synthesized to form the complete load-displacement curve (Figure 8b).

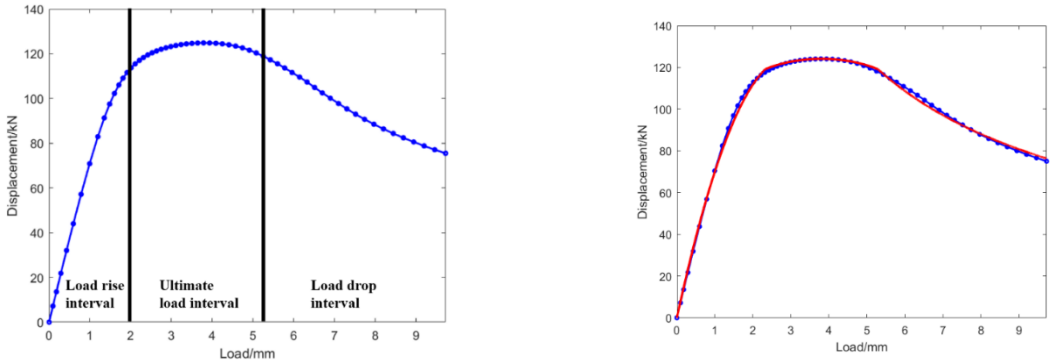

(a). Load-displacement curve segments. (b). Load-displacement curve fitting.

Figure 8. The process of segmenting fitting for the load-displacement curve.

$$y_1 = ax_1^2 + bx_1 \tag{9}$$

$$(x_2 - o_x)^2 + \left(y_2 - o_y\right)^2 = r^2 \tag{10}$$

$$y_3 = mx_3^n \tag{11}$$

5 CONCLUSIONS

This paper analyzes 100 numerical models of Cee-shape CFS axial compression members based on the traditional buckling modal analysis. Using linear regression on this database, a surrogate model, FTM is established that can predict the peak load based on the initial geometric characteristics of the numerical model. The model is then discussed and analyzed.

(1) A thorough examination of the correlation between the initial geometric parameters of the numerical model and the analysis outcomes identifies three pivotal geometric parameters: thickness, slenderness ratio, and web height to thickness ratio.

(2) The database is partitioned, with 80% of the sample data serving as the training set for the machine learning surrogate model, and the remaining 20% used to assess the model's

performance. The FTM model is derived by setting a threshold, yielding an average error of 6.7% for the testing set.

(3) The model undergoes validation using the entire sample data, yielding relatively accurate predictions. The discrepancies and ratios between predicted and actual loads adhere to a normal distribution. The model's performance is further evaluated using a variety of metrics, including mean square error (MSE), coefficient of determination (R^2), and coefficient of variation (COV) between predicted and target values. These results underscore the model's proficiency in predicting the ultimate load, along with benefits such as rapid training speed and ease of comprehension.

The study also offers insightful recommendations for machine learning applications in the complete force process of axial compression numerical models, encompassing load-displacement curves. It proposes segmented fitting based on load-displacement curve characteristics and parameterizes individual segmented regions. Furthermore, a proxy model is suggested to predict curve parameters, drawing on the training experience with the surrogate model. By fitting the curve parameters, a proxy model capable of predicting the complete force process is achieved. This approach introduces novel perspectives for predicting and analyzing the complete force process of Cee-shaped CFS members.

REFERENCES

[1] B. Lechner and M. Pircher, "Analysis of imperfection measurements of structural members," Thin-walled structures, vol. 43(3), pp. 351-374, 2005.

[2] H. Amouzegar, B. Amirzadeh, X. Zhao, B. Schafer and M. Tootkaboni, "Statistical analysis of the impact of imperfection modes on collapse behavior of cold-formed steel members," In Proceedings of Structural stability Research Council Annual Sta, 2015.

[3] H. S. Ahmed, S. Ghosh and M. Mangal, "Probabilistic estimation of the buckling strength of a CFS lipped-channel section with Type 1 imperfection," Thin-Walled Structures, vol. 119, pp. 447-456, 2017.

[4] V. M. Zeinoddini and B. W. Schafer, "Simulation of geometric imperfections in cold-formed steel members using spectral representation approach," Thin-Walled Structures, vol. 60, pp. 105-117, 2012.

[5] "AISI S240-15.North American Standard for Cold Formed Steel Structural Framing.," 2015.

[6] P. Feng, Y. Zou, L. Hu and T. Liu, "Use of 3D laser scanning on evaluating reduction of initial geometric imperfection of steel column with pre-stressed CFRP," Engineering Structures, vol. 198(109527), 2019.

[7] X. Zhao, M. Tootkaboni and B. Schafer, "Laser-based cross-section measurement of cold-formed steel members: Model reconstruction and application," Thin-Walled Structures, vol. 120, pp. 70-80, 2017.

[8] X. Zhao, G. Wang, X. Sun, X. Wang and B. Schafer, "Modeling of uncertain geometry of cold formed steel members based on laser measurements and machine learning," Engineering Structures, vol. 115578, p. 279, 2023.

[9] "Geomagic version 2013.0.2 [Computer software]. Geomagic, Inc. and 3Dsystems. Inc. Mole".

[10] Y. LeCun , Y. Bengio and G. Hinton, "Deep learning," nature, vol. 521(7553), pp. 436-444., 2015.

[11] I. Goodfellow, Y. Bengio and A. Courville, "Deep learning," MIT press, 2016.

[12] Y. Xu, B. Zheng and M. Zhang, "Capacity prediction of cold-formed stainless steel tubular columns using machine learning methods," Journal of Constructional Steel Research, vol. 106682, p. 182, 2021.

[13] L. Xiao, Q. Li, H. Li and Q. Ren, "Loading capacity prediction and optimization of cold-formed steel built-up section columns based on machine learning methods," Thin-Walled Structures, vol. 109826, p. 180, 2022.

[14] M. Dissanayake, H. Nguyen and K. Poologanathan, "Prediction of shear capacity of steel channel sections using machine learning algorithms," Thin-Walled Structures, vol. 109152, p. 175, 2022.

[15] Z. Sun, Y. Zheng, Y. Sun, X. Shao and G. Wu, "Deformation ability of precast concrete columns reinforced with steel-FRP composite bars (SFCBs) based on the DIC method," Journal of Building Engineering, vol. 106083, p. 68, 2023.

[16] Q. Tong, C. Couto and T. Gernay, "Machine learning models for predicting the resistance of axially loaded slender steel columns at elevated temperatures," Engineering Structures, vol. 114620, p. 266, 2022.